Bo Yu (ed.) (2012). *2012 IEEE Nuclear Science Symposium and Medical Imaging Conference (NSS/MIC): Anaheim, California, USA. October 29 - November 3, 2012* . IEEE, 3835-3838 .
DOI: http://dx.doi.org/10.1109/NSSMIC.2012.6551880

Complete scheme for beam hardening correction in small animal computed tomography

C. de Molina, A. Sisniega, J.J. Vaquero, *Member, IEEE*, M. Desco and M. Abella

***Abstract*–. CT images are often affected by beam hardening artifacts due to the polyenergetic nature of the X-ray beam. Several correction methods have been proposed to be included in an FDK reconstruction scheme, which is still the prefered reconstruction algorithm in commercial X-ray CT scanners.**

In this work, we present a complete correction scheme for beam hardening artifact correction in an FDK-based reconstruction scenario that accounts for both cupping artifact and dark streaks. The proposed method substitutes the need of the knowledge of the spectrum by empirical measurements and two parameters. It includes two steps: a linearization step of projection data and a post-reconstruction step. Evaluation done in real studies acquired with a cone-beam micro-CT scanner showed an average cupping reduction of 80 % in homogeneous phantoms and 72% in rodent studies. The correction scheme can be incorporated easily in any cone beam micro-CT scanner.

I. Introduction

The origin of the beam hardening phenomenon in X-ray tomographs lies in the polychromatic nature of the source spectrum. We can define beam hardening as the process by which the mean energy of the X-ray beam increases with the amount of traversed material (the beam is hardened) due to the fact that the lower energy photons are preferably absorbed.

In the case of an ideal X-ray source, the measured intensity by the detector is directly proportional to the traversed material thickness. Nevertheless, in a real X-ray source (with a polychromatic beam), this relationship is non-linear, due to the dependence of the attenuation coefficient with the energy. This produces incoherent data and consequently, artifacts in the reconstructed images.

The most common artifacts originated by beam hardening are cupping in homogeneous volumes and streaks (dark bands) between dense objects like bone [1]. Both artifacts hinder the qualitative and quantitative analysis of the CT images.

There are different correction schemes proposed in the literature. Usually, a filter [2] is included in most of commercial scans between the source and the sample to pre-harden the beam, but it is not sufficient to eliminate the beam hardening artifacts. The linearization method [2-4] corrects the cupping artifact in homogeneous volumes but is insufficient for eliminating the dark streaks present between dense objects like bones.

Other strategies like dual energy [5, 6], post-processing [7-9] and reconstruction with iterative methods [10-12] have been proposed. The main drawbacks of these approaches are that the dual energy technique requires a sophisticated hardware and more radiation dose and the iterative methods involve high computational burden.

We present a complete correction scheme for beam hardening artifact correction in an FDK based reconstruction scenario based on the work of Joseph and Spital [7]. It accounts for both cupping artifact and dark streaks while avoiding the need of the knowledge of the source spectrum.

II. Materials and Methods

The proposed scheme (Fig. 1) includes two corrections: a linearization of projection data and a post-reconstruction correction.

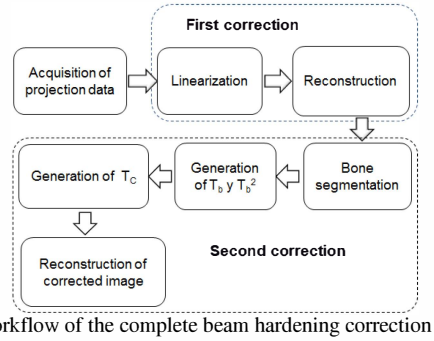

Fig. 1. Workflow of the complete beam hardening correction scheme.

The first correction assumes the sample is homogenous and with attenuation properties similar to water. In a calibration phase, we calculate the linearization function, $T(t_w)$, that converts the total attenuation for the polychromatic case (beam hardening function) into the total attenuation for the equivalent monochromatic case (ideal function) shown in Fig. 2.

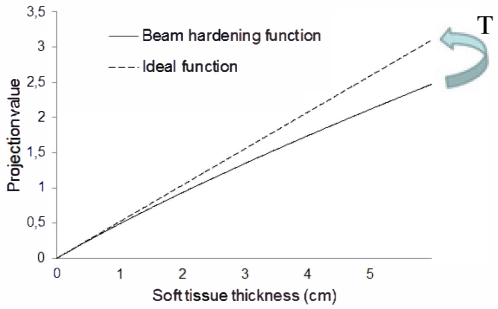

Fig. 2. Beam hardening and ideal function versus different thicknesses of water.

This work was supported in part by projects TEC2008-06715 and TEC2007-64731 (Ministerio de Ciencia e Innovación), EU-FP7 FMTXCT-201792, ARTEMIS S2009/DPI-1802 (Comunidad de Madrid), and European Regional Development Funds (FEDER) and CDTI under the CENIT program (AMIT project, CEN20101014).

All authors are with the Departamento de Bioingeniería e Ingeniería Aeroespacial, Universidad Carlos III, Madrid, Spain (e-mail: monica.abella@uc3m.es).

Manuel Desco and Juan José Vaquero are with the Instituto de Investigación Sanitaria Gregorio Marañón (IiSGM), Madrid, Spain.

Manuel Desco is with the Centro de Investigación en Red de Salud Mental (CIBERSAM, CIBER CB07/09/0031), 28007 Madrid, Spain.

The calibration process, consisting of three steps, has to be done for every tube voltage and filter used in the scanner. First, to empirically obtain values of the beam hardening function, F_{BH} (t_w), for different traversed thickness of water (avoiding the knowledge of spectrum), we acquire the calibration phantom shown in Fig. 3, left. To generate the vector of traversed thicknesses (t_w, soft tissue thickness in Fig. 2), the data is reconstructed with an FDK-based algorithm [1] and a mask is created by thresholding and then projected (Fig. 3, right).

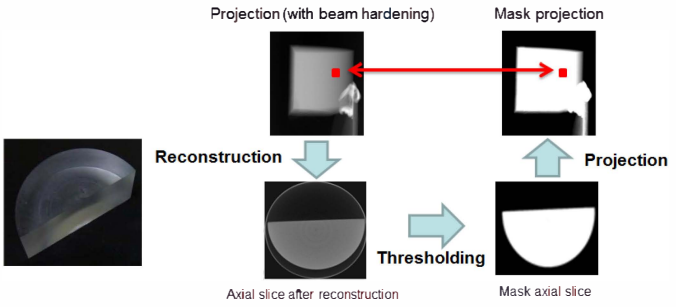

Fig. 3. Polymetilmetacrilate semi-cylinder, with attenuation characteristics similar to soft tissue, used as calibration phantom (left). Work-flow of the first step of the calibration process to obtain the beam hardening function from the acquisition data of the calibration phantom (right).

Secondly, the ideal function is obtained by calculating the tangent to the first part of the beam hardening function (obtained with 4 % of the total points).

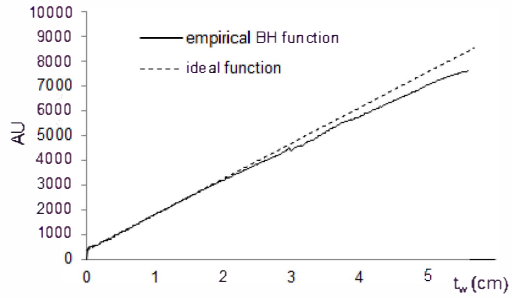

Fig. 4. Beam hardening function obtained experimentally and ideal function obtained as its tangent.

Finally, the linearization function, $T(t_w)$ is obtained and fitted to a third order polynomial:

$$T(t_w) = at_w^3 + bt_w^2 + ct_w + d, \text{ with } t_w = \int_L \rho_w \cdot dl\,, \quad (1)$$

where ρ_w is the water density and L is the ray path length.

This first correction, consisting on applying the function $T(t_w)$ to the projection data, is not sufficient for correcting the dark streaks between dense parts like bones in laboratory rodents.

If we estimated that small animal is composed of two materials (soft tissue and bone), one option for a complete correction could be to obtain the 2D beam hardening function for different combinations of these two materials (like the simulation shown in Fig. 5) and to use the same strategy as explained above. Nevertheless, obtaining this 2D function empirically (without the knowledge of the emitted spectrum) is cumbersome.

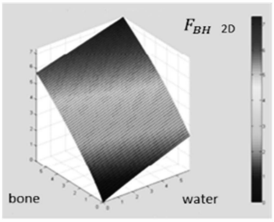

Fig. 5. Beam hardening function for different combinations of bone and water.

For the second correction, we make use of the idea outlined in [7]: to transform the whole sample into "equivalent water" and to use the linearization function $T(t_w)$ obtained before. To this end, we need to find the amount of water that would have attenuation properties equivalent to each combination of water and bone traversed, so that

$$F_{BH\,2D}(t_w, t_b) = F_{BH\,2D}(t_w + \sigma(t_w, t_b), 0) = F_{BH\,1D}(t_e) \quad (2)$$

where the line integral of the equivalent water path is given by $t_e = t_w + \sigma(t_w, t_b)$.

Following the ideas in [7, 12, 13], we approximate $\sigma(t_w, t_b)$ to a second order polynomial only dependent on the amount of bone traversed by the X-rays:

$$\sigma(t_w, t_b) = At_b - Bt_b^2 \quad (3)$$

The correction is done in the projection space as:

$$proj_{corr} = proj_{line} + \mathrm{A} \cdot proj_{b\_line} + \mathrm{B} \cdot proj_{b\_line}^2 \quad (4)$$

where $proj_{corr}$ is the corrected projection data, $proj_{line}$ is the linearized projection data, $proj_{b\_line}$ is the bone projection data, and A and B are constants obtained empirically. To obtain $proj_{b\_line}$, the bone part is segmented from a previously reconstructed image and then projected. The value of B affects the correction of the streaks and the quantification in bone areas and A is responsible of restoring the correct quantification in bone.

A. Beam hardening simulations

We studied the dependency of the A and B parameters with the characteristics of the acquisition (X-ray source voltage and current) and the size of the sample. To this end, we simulated the acquisition process including beam hardening effect using the IRT toolbox developed by the University of Michigan (http://web.eecs.umich.edu/~fessler/code/index.html).

To study the voltage dependence, we used an ellipsoidal phantom made of soft tissue with two cylindrical bone inserts (Fig. 6).

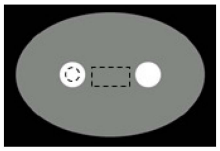

Fig. 6. Ellipsoidal phantom made of soft tissue with 30 cm and 20 cm diameter sizes and two bone inserts with 4 cm diameter. Dotted lines indicate areas used for measurements.

In order to choose the optimum B and A parameters, we corrected the phantom with different values and quantified the difference with a reference image (monoenergetic

reconstruction) in terms of the mean square error (MSE). To search the optimum value for B, MSE is calculated for the rectangle between the bone parts and, for the case of A, in the circular area shown in Fig. 6.

Fig. 7 shows an example of the cost function when looking for the optimum value of the B parameter.

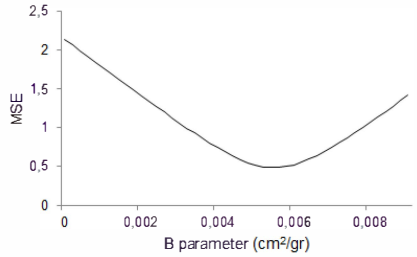

Fig. 7. Example of cost function for different B values for the 100 KVp case (MSE measured in the rectangular area is shown Fig. 6).

X-ray current does not affect the beam hardening artifact. When varying the X-ray source voltage between 80-140 KVp (typical values for the human studies), B does not change but A increases with the voltage (Fig. 8, right).

We also studied the dependency of A and B parameters with the size of bone in the sample. We modified the diameter of the bone inserts between 3 cm and 6 cm and obtained an increase of A for larger bones as shown in Fig. 8, left. On the other hand, B was found to be independent of the amount of bone.

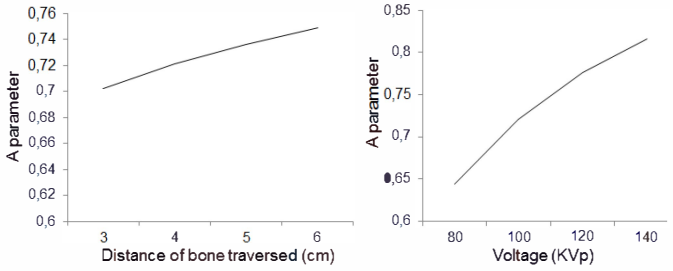

Fig. 8. Dependency of the optimum value of A with the distance of bone traversed (left) and the source voltage (right).

We quantified the dependence of the beam hardening artifact with characteristics of the source in a small-animal scenario with a high resolution CT. To this end, we used a cylindrical phantom made of soft tissue of 6 cm diameter. We can see in Fig. 9 a dependence of the beam hardening artifact with both source voltage and sample size (it increases with the size of the tissue traversed and decreases as the voltage increases).

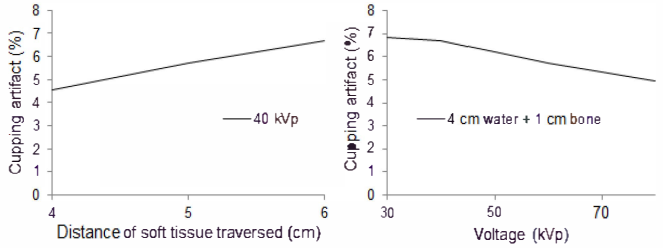

Fig. 9. Dependency of the cupping artifact with the distance of tissue traversed (left) and with the source voltage (right) for the small-animal scenario.

B. *Assessment of performance in real data*

The proposed correction scheme was evaluated on real studies acquired with a cone-beam micro-CT scanner [14]:

- Three polymethylmethacrylate cylinders with 3, 4, and 6 cm diameter.
- A two-density cylindrical phantom of 3 cm diameter filled with water with two cylinders inside filled with iodine solution (60% iodine/40% saline).
- Three rodent studies.

Acquisition parameters were 40 KVp-45 KVp, 200 µA, 2 mm aluminum filter, 360 projections, binning 4, and 8 shots (values typically used in the scanner for pre-clinical research).

We quantified the cupping reduction as:

$$CR = \frac{P_1 - P_C}{P_1 - P_A} \cdot 100\% \quad (5)$$

where P_1 is the point of minimum beam hardening effect (at the edges of the cylinder), P_C is the point of maximum artifact (at the center of the cylinder) and P_A is the background value, as shown in Fig. 10.

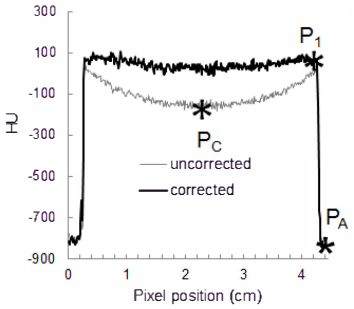

Fig. 10. Profiles of the reconstruction of a homogeneous phantom before and after the first step of the correction

We quantified dark streaks reduction using the perpendicular profile to each streak (see Fig. 11) by:

$$ANR = \frac{(\mu_{corr} - min_{uncorr})}{\sigma} \quad (6)$$

where ANR is the Artifact-Noise Ratio, μ_{corr} is the mean profile in the correct image, min_{uncorr} is the minimum value of the profile in the uncorrected image and σ is the standard deviation in a homogeneous area.

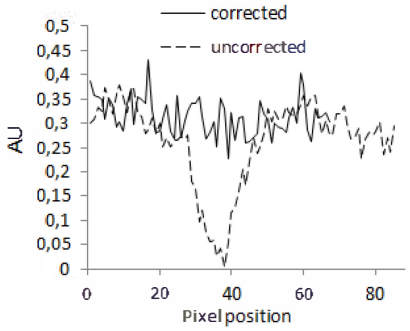

Fig. 11. Corrected and uncorrected profiles perpendicular to the dark streak.

III. RESULTS AND CONCLUSIONS

Fig. 12 shows the results of applying the proposed correction scheme in real studies. Cupping and streaks artifacts are noticeably reduced.

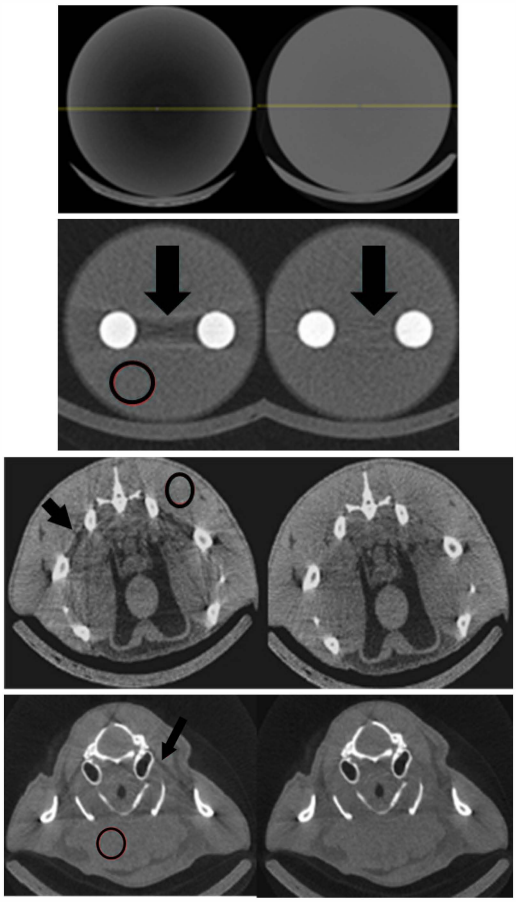

Fig. 12. Central slice of reconstructed images before (left) and after beam-hardening correction with the proposed scheme. The lines in the top image indicate where the profiles to calculate CR were taken. The black circles indicate the homogenous areas in which we measured the noise for equation (6).

The quantitative results are shown in the Table 1, with a mean cupping reduction in homogenous cylinders of 79 % and a mean streak reduction of 72 %.

TABLE I. RESULTS IN REAL DATA

Study	Voltage (KVp)	Art. red (%)	A	B
3cm-cylinder	45	95.53	-	-
4cm cylinder	45	77.02	-	-
6cm cylinder	45	78.94	-	-
2-material	40	68	0.92	0.032
rat pelvis	45	74	0.83	0.032
rat skull	45	72	0.90	0.032

I. DISCUSSION

We have proposed a complete scheme for beam-hardening correction in CT. The method includes two corrections: a linearization of projection data for eliminating cupping artifacts and a post-processing correction on the reconstructed image for streak reduction. The results of our evaluation demonstrate the effectiveness of the proposed beam hardening correction scheme in a small-animal scanner.

The method substitutes the need of the knowledge of the spectrum by empirical measurements and two parameters, A and B, calculated heuristically. B is responsible for the streak artifacts and does not depend on source voltage or sample size. A is responsible of restoring the quantitative value in bone and has to be obtained for each voltage and sample size.

Since it is based on empirical measurements, we expected to correct the artifacts derived from scattering.

The proposed calibration scheme has been incorporated in the ARGUS-CT scanner and could be easily adapted to any other cone beam micro-CT scanner. To incorporate the algorithm in a scanner it is only necessary to calibrate the beam hardening function for water and to build a look-up table with A and B values.

REFERENCES

[1] J. F. Barrett and N. Keat, "Artifacts in CT: Recognition and Avoidance," *RadioGraphics,* vol. 24, pp. 1679-1691, 2004.

[2] R. A. Brooks and G. D. Chiro, "Beam hardening in x-ray reconstruction tomography," *Phys. Med. Biol.,* vol. 21, pp. 390-8, 1976.

[3] G. T. Herman, "Correction for beam hardening in computed tomography," *Phys. Med. Biol.,* vol. 24, pp. 81-106, 1979.

[4] W. D. McDavid*, et al.*, "Correction for spectral artifacts in cross-sectional reconstruction from X-rays," *Med. Phys.,* vol. 4, pp. 54–7, 1997.

[5] P. Sukovic and N. H. Clinthorne, "Design of an experimental system for dual energy x-ray CT," in *IEEE Nuclear Science Symposium Conference Record*, 1999, pp. 1021-1022.

[6] J. A. Fessler*, et al.*, "Maximum-likelihood dual-energy tomographic image reconstruction," *Proc. SPIE,* vol. 4684, pp. 38-49, 2002.

[7] P. M. Joseph and R. D. Spital, "A method for correcting bone induced artifacts in computed tomography scanners," *J. Comp. Assisted Tomo.,* vol. 2, pp. 100-8, 1978.

[8] O. Nalcioglu and R. Y. Lou, "Post-reconstruction Method for Beam Hardening in Computerised Tomography," *Phys. Med. Biol.,* vol. 24, pp. 330-40, 1979.

[9] P. M. Joseph and C. Ruth, "A method for simultaneous correction of spectrum hardening artifacts in CT images containing both bone and iodine," *Med. Phys.,* vol. 24, pp. 1629-34, 1997.

[10] B. De Man*, et al.*, "An Iterative Maximum-Likelihood Polychromatic Algorithm for CT," *IEEE Trans. Med. Imaging,* vol. 20, pp. 999-1008, 2001.

[11] I. A. Elbakri and J. A. Fessler, "Statistical Image Reconstruction for Polyenergetic X-Ray Computed Tomography," *IEEE Trans. Med. Imaging,* vol. 21, pp. 89-99, 2002.

[12] M. Abella and J. A. Fessler, "A new statistical image reconstruction algorithm for polyenergetic X-ray CT," *Proceedings of the 2009 IEEE International Symposium on Biomedical Imaging (ISBI),* pp. 165-8, 2009.

[13] J. Hsieh*, et al.*, "An iterative approach to the beam hardening correction in cone beam CT," *Med. Phys.,* vol. 27, pp. 23-29, 2000.

[14] J. J. Vaquero*, et al.*, "Assessment of a New High-Performance Small-Animal X-ray Tomograph," *IEEE Trans. Nucl. Sci.,* vol. 55, pp. 898-905, 2008.